Multiplicity distribution in ultrarelativistic nucleus-nucleus collisions

S. Daté and D. Kiang
Department of Physics, Dalhousie University, Halifax, Nova Scotia, Canada B3H 3J5

C. K. Chew*
International Centre for Theoretical Physics, I-34100 Trieste, Italy
(Received 12 May 1987)

Charged secondary multiplicity distributions for various nucleus-nucleus collisions at 200 and 15 GeV/nucleon are calculated based on the hypothesis of universal Koba-Nielsen-Olesen scaling at each impact parameter. The correlation between the multiplicity cut and the cut in impact parameter is also discussed.

I. INTRODUCTION

There is a great deal of interest in ultrarelativistic nucleus-nucleus collisions in recent years,[1-3] and experimental programs[3] are being carried out at CERN and BNL. The experiments in CERN use ^{16}O and ^{32}S as the projectiles bombarding fixed nuclear targets at an incident laboratory energy per nucleon, $E_{\rm lab}$, of 200 GeV/nucleon. The NA35 group[4] in CERN, using the ^{16}O beam, observed a wide transverse-energy (E_T) distribution for particles produced in $2.2 \leq y \leq 3.8$ and a large $\langle E_T/\text{particle} \rangle$ value among those particles in $60 \leq E_T \leq 80$ GeV. Experiments in BNL will use a variety of projectiles at $E_{\rm lab} \leq 28$ GeV/nucleon.

One of the most interesting aspects in ultrarelativistic nucleus-nucleus collisions is the possibility to observe the formation of the quark-gluon-plasma (QGP) phase. Formation of the QGP may be revealed through[1-3] an excess of dileptons, direct photons, strange particles, and an enhancement of p_t or E_T per particle. These and other signals of new phenomena will be pronounced in high-multiplicity events. In fact, the occurrence of new phenomena has been suggested in association with high-multiplicity events in cosmic-ray experiments.[5] Since almost all of the theoretical calculations for signals of the QGP are done for central collisions, it is desirable to correlate multiplicities with the impact parameter (b_I) of colliding nuclei when comparing theoretical predictions with experimental data. Furthermore, there is speculation that hadronization of QGP will produce a large excess of entropy.[6] A large entropy production will affect the multiplicity distribution at high multiplicities.

Another point of interest in ultrarelativistic nucleus-nucleus collisions is the comparison of models of particle production built for hadron-nucleus collisions. Among several models, the multichain model[7,8] (MCM) and the wounded-nucleon model[9,10] (WNM) predict considerably different mean multiplicities[8] for collisions of heavy nuclei at high energies when the cascading effect in projectile nuclei is neglected.

The aim in this paper is to present a simple and coherent model of the multiplicity distribution in ultrarelativistic nucleus-nucleus collisions and to make predictions based on the knowledge of hadron-hadron and hadron-nucleus collisions. Since, in the CERN experiment,[4] the spectator nucleons in the beam nucleus are thrown into the veto calorimeter and those in the target nucleus can be removed by cuts in the laboratory angles of the produced particles, we concentrate on the multiplicities of the secondary (or participant) particles which include wounded nucleons in the colliding nuclei and particles produced in collisions of those nucleons. In some previous papers,[11] the multiplicity distribution was calculated as an explicit sum of the contributions from individual nucleon-nucleon collisions. This method becomes, however, formidable when the colliding nuclei are large and $E_{\rm lab}$ is large. To overcome this difficulty, we employ an empirical rule which is satisfied by the multiplicity distribution of the secondary particles for nucleon-nucleon and nucleon-nucleus collisions. It was shown[12] that the hypothesis of universal Koba-Nielsen-Olesen (KNO) scaling at each impact parameter leads to a satisfactory agreement between calculations and experimental data[13] on $p + \text{Ar}$ and $p + \text{Xe}$ collisions at 200 GeV. The predicted target-mass number dependence was further confirmed[14] in a recent experiment with Mg, Ag, and Au as targets bombarded by 100-GeV hadrons. In this paper, we apply the same hypothesis to nucleus-nucleus collisions.

An important feature of our model is that, once the mean multiplicity $\langle n(b_I, E_{\rm lab}) \rangle_{AB}$ in collisions of nuclei A and B as a function of b_I is given, our model contains no free parameter. That is described in Sec. II. As shown in Sec. III, the KNO function $\psi_{AB}(z, E_{\rm lab})$ for all nucleus-nucleus collisions is a useful vehicle for comparison with experiments.

II. THE MODEL

We regard $A + B$ collisions, in which the production of secondary particles occurs, as proceeding in two stages: In the first stage, multiple collisions among participant nucleons take place and spectator nucleons decouple from the interaction. In the subsequent stage, the secondary particles are produced via intermediate products formed by the multiple collisions among the participant nucleons. The assumptions of our model are as follows.

(1) The first stage is described by the Glauber theory which has been extended to $A+B$ collisions.[9,15]

(2) The second stage is independent of the first stage: If the same intermediate products were formed in different reactions, the spectra of the secondary particles are the same.

(3) The multiplicity n of charged secondary particles produced from the intermediate products obeys a distribution which is parametrized by only one parameter: namely, the mean multiplicity. This distribution is universal for all $A+B$ collisions including $N+N$ and $N+B$ collisions.

Since KNO scaling is valid for $N+N$ collisions below $Sp\bar{p}S$ energies, the last assumption (3) implies that the universal multiplicity distribution P_n for a fixed mean multiplicity $\langle n \rangle$ can be written as

$$P_n=(1/\langle n \rangle)\psi(n/\langle n \rangle) \tag{2.1}$$

with

$$\psi(z)=\langle n(E_{\rm lab})\rangle_{NN}\sigma_{n'}^{NN}(E_{\rm lab})/\sigma_{\rm inel}^{NN} ,$$
$$n'=z\langle n(E_{\rm lab})\rangle_{NN} , \tag{2.2}$$

where $\langle n(E_{\rm lab})\rangle_{NN}$ is the mean charged multiplicity, and $\sigma_{n'}^{NN}(E_{\rm lab})$ and $\sigma_{\rm inel}^{NN}$ are the n'-charged-prong and total inelastic cross sections, respectively, in $N+N$ collisions at $E_{\rm lab}$. For $A+B$ collisions, $\langle n \rangle$ in Eq. (2.1) is given as a function of the overall impact parameter b_I and laboratory energy per nucleon $E_{\rm lab}$, $\langle n(b_I,E_{\rm lab})\rangle_{AB}$, and we write Eq. (2.1) as

$$P_n^{AB}(b_I,E_{\rm lab})=[1/\langle n(b_I,E_{\rm lab})\rangle_{AB}]\times\psi(n/\langle n(b_I,E_{\rm lab})\rangle_{AB}) . \tag{2.3}$$

Assumptions (1) and (2) then imply that the multiplicity distribution in $A+B$ collisions is given by

$$P_n^{AB}=\int d^2b_I\frac{\sigma_{\rm abs}^{AB}(b_I)}{\sigma_{\rm abs}^{AB}}P_n^{AB}(b_I,E_{\rm lab}) , \tag{2.4}$$

where the weight $\sigma_{\rm abs}^{AB}(b_I)/\sigma_{\rm abs}^{AB}$ for collisions at b_I is given in the Glauber theory.[9,15]

We note that our model contains no free parameter once $\langle n(b_{I,b_{\rm lab}})\rangle_{AB}$ is given. With point nucleons, our model, for the case of $B=N$, reduces to the model of Ref. 12, and reduces to $N+N$ collisions for the case of $A=N$ and $B=N$.

We define the KNO function for $A+B$ collisions by

$$\psi_{AB}(z,E_{\rm lab})=\langle n(E_{\rm lab})\rangle_{AB}P_n^{AB}=\int d^2b_I\frac{\sigma_{\rm abs}^{AB}(b_I)}{\sigma_{\rm abs}^{AB}}Q_{AB}^{-1}(b_I,E_{\rm lab})\times\psi(zQ_{AB}^{-1}(b_I,E_{\rm lab})) , \tag{2.5}$$

where

$$n=z\langle n(E_{\rm lab})\rangle_{AB} ,$$
$$\langle n(E_{\rm lab})\rangle_{AB}=\int d^2b_I\frac{\sigma_{\rm abs}^{AB}(b_I)}{\sigma_{\rm abs}^{AB}}\langle n(b_I,E_{\rm lab})\rangle_{AB} , \tag{2.6}$$

and

$$Q_{AB}(b_I,E_{\rm lab})=\langle n(b_I,E_{\rm lab})\rangle_{AB}/\langle n(E_{\rm lab})\rangle_{AB} . \tag{2.7}$$

In the second equation of Eq. (2.5), we have used Eqs. (2.3) and (2.4). We easily observe that $\psi_{AB}(z,E_{\rm lab})$ scales with energy if $Q_{AB}(b_I,E_{\rm lab})$ is energy independent and the weak energy dependence of $\sigma_{\rm abs}^{AB}(b_I)/\sigma_{\rm abs}^{AB}$ is ignored.

We must now determine $\langle n(b_I,E_{\rm lab})\rangle_{AB}$. The WNM (Ref. 10) gives the charged secondary multiplicity as

$$\langle n(b_I,E_{\rm lab})\rangle_{AB}=[\langle w_A(b_I)\rangle+\langle w_B(b_I)\rangle]\times\langle n(E_{\rm lab})\rangle_{NN}/2 , \tag{2.8}$$

where $\langle w_A(b_I)\rangle$ [$\langle w_B(b_I)\rangle$] is the average number of wounded nucleons in the nucleus A [B]. We note that the contribution from the spectator nucleons is not included in Eq. (2.8). Because of the factorizable nature of Eq. (2.8), the energy dependence in $Q_{AB}(b_I,E_{\rm lab})$ cancels out, and as mentioned before, $\psi_{AB}(z,E_{\rm lab})$ scales approximately with energy. Another form of $\langle n(b_I,E_{\rm lab})\rangle_{AB}$ is provided by the MCM (Ref. 8) as

$$\langle n(b_I,E_{\rm lab})\rangle_{AB}=\langle N_{AB}(b_I)\rangle\langle n[\Gamma_{AB}(b_I)E_{\rm lab}]\rangle_{NN} , \tag{2.9}$$

$$\Gamma_{AB}^{-1}(b_I)=\langle \nu_A(b_I)\rangle\langle \nu_B(b_I)\rangle , \tag{2.10}$$

where $\langle N_{AB}(b_I)\rangle$ denotes the average total number of $N+N$ collisions for $A+B$ collisions at b_I, and $\langle \nu_A(b_I)\rangle$ [$\langle \nu_B(b_I)\rangle$] is the average collision number of a wounded nucleon in the nucleus B [A]. In Eq. (2.9), we have adopted the simplest model (which is case I of Ref. 8) of the equipartition for the collision energy-momentum among $N+N$ collisions. It is seen that the energy dependence of $Q_{AB}(b_I,E_{\rm lab})$ cancels out if $\langle n(E_{\rm lab})\rangle_{NN}$ obeys a power law. In reality, it does not, and therefore $\psi_{AB}(z,E_{\rm lab})$ will not scale. It turns out that at 200 GeV/nucleon, for large z, $\psi_{AB}(z,E_{\rm lab})$ is quite independent of the particular choice of $\langle n(b_I,E_{\rm lab})\rangle_{NN}$. In the following, we call those choices of $\langle n(b_I,E_{\rm lab})\rangle_{NN}$ case WNM and case MCM, respectively.

We summarize the formulas of the Glauber theory extended[9,15] to nuclear collisions. The absorption cross section is given by

$$\sigma_{\rm abs}^{AB}=\int d^2\mathbf{b}_I\sigma_{\rm abs}^{AB}(b_I) , \tag{2.11}$$

where

$$\sigma_{\rm abs}^{AB}(b_I)=1-\left[1-\int d^2\mathbf{b}\,\sigma_{\rm inel}^{NN}t_A(\mathbf{b})t_B(\mathbf{b}_I+\mathbf{b})\right]^{AB} , \tag{2.12}$$

$$t_A(\mathbf{b})=\int dz\,\rho_A(z,\mathbf{b}) , \tag{2.13}$$

with $\rho_A(z,\mathbf{b})$ being the nuclear density for the nucleus A and normalized to unity. In Eq. (2.8), we use

$$\langle w_A(b_I)\rangle = [A/\sigma_{\rm abs}^{AB}(b_I)] \times \int d^2\mathbf{b}\, t_A(\mathbf{b})\{1-[1-\sigma_{\rm inel}^{NN} t_B(\mathbf{b}_I+\mathbf{b})]^B\} \tag{2.14}$$

and a similar expression for $\langle w_B(b_I)\rangle$. In Eq. (2.10), we use

$$\langle \nu_A(b_I)\rangle = [A/\sigma_A(b_I)] \times \int d^2\mathbf{b}\, \sigma_{\rm inel}^{NN} t_A(\mathbf{b}) t_B(\mathbf{b}_I+\mathbf{b}) , \tag{2.15}$$

where

$$\sigma_A(b_I) = \int d^2\mathbf{b}\, t_B(\mathbf{b})\{1-[1-\sigma_{\rm inel}^{NN} t_A(\mathbf{b}_I+\mathbf{b})]^A\} , \tag{2.16}$$

and a similar expression for $\langle \nu_B(b_I)\rangle$. $\langle N_{AB}(b_I)\rangle$ in Eq. (2.9) is related to these quantities by

$$\langle N_{AB}(b_I)\rangle = \langle w_A(b_I)\rangle\langle \nu_B(b_I)\rangle = \langle w_B(b_I)\rangle\langle \nu_A(b_I)\rangle . \tag{2.17}$$

III. NUMERICAL RESULTS

A. Input

We use the following input for our model.

(a) For the KNO scaling function ψ in Eqs. (2.3) and (2.5), we use the parametrization given by Slattery:[16]

$$\psi(z) = \tfrac{1}{2}(3.79z + 33.7z^3 - 6.64z^5 + 0.332z^7)\exp(-3.04z) . \tag{3.1}$$

(b) For $\langle n(E_{\rm lab})\rangle_{NN}$ in Eqs. (2.8) and (2.9), we write

$$\langle n(E_{\rm lab})\rangle_{NN} = \langle n(E_{\rm lab})\rangle_{pp} - 1 , \tag{3.2}$$

where we regard approximately half of the incident nucleons coming from colliding nuclei as neutral. The mean charged multiplicity in pp collisions, $\langle n(E_{\rm lab})\rangle_{pp}$, is given by[17]

$$\langle n(E_{\rm lab})\rangle_{pp} = 1.20 + 0.589\ln(E_{\rm lab}) + 0.118[\ln(E_{\rm lab})]^2 , \tag{3.3}$$

where $E_{\rm lab}$ is in units of GeV.

TABLE I. Calculated values of $\sigma_{\rm abs}^{AB}$, $\langle w_A\rangle$, $\langle w_B\rangle$, and $\langle N_{AB}\rangle$ at $E_{\rm lab}=200$ GeV/nucleon. Also shown are values of $\langle n(E_{\rm lab})\rangle_{AB}$ calculated using the MCM and WNM at 200 GeV/nucleon. Values in parentheses are those for $E_{\rm lab}=15$ GeV/nucleon.

$A+B$	$\sigma_{\rm abs}^{AB}$ (mb)	$\langle w_A\rangle$	$\langle w_B\rangle$	$\langle N_{AB}\rangle$	$\langle n(E_{\rm lab})\rangle_{AB}$ MCM	WNM
^{16}O + ^{207}Pb	3623	7.62	15.9	29.4	101	78.2
	(3582)	(7.56)	(15.4)	(27.3)	(22.1)	(31.4)
^{16}O + ^{108}Ag	2676	6.60	11.2	20.8	77.2	59.3
	(2641)	(6.53)	(10.9)	(19.3)	(18.9)	(23.8)
^{16}O + ^{56}Fe	1995	5.58	7.82	14.4	58.0	44.5
	(1963)	(5.50)	(7.60)	(13.5)	(15.5)	(17.9)
^{16}O + ^{16}O	1169	3.81	3.81	7.03	31.9	25.3
	(1144)	(3.72)	(3.72)	(6.61)	(9.62)	(10.2)
^{32}S + ^{207}Pb	4306	12.8	22.4	49.5	158	117
	(4263)	(12.7)	(21.8)	(45.9)	(31.2)	(47.2)
^{32}S + ^{108}Ag	3267	10.8	15.4	34.0	118	87.0
	(3228)	(10.7)	(15.0)	(31.6)	(26.6)	(35.2)
^{32}S + ^{56}Fe	2507	8.88	10.4	23.0	86.3	64.0
	(2473)	(8.73)	(10.1)	(21.4)	(21.5)	(25.8)
^{32}S + ^{16}O	1565	5.69	4.75	10.5	44.7	34.7
	(1537)	(5.54)	(4.66)	(9.84)	(12.7)	(14.0)
^{207}Pb + ^{207}Pb	7464	47.9	47.9	185	462	318
^{108}Ag + ^{108}Ag	4817	24.8	24.8	77.9	235	165
^{56}Fe + ^{56}Fe	3046	12.8	12.8	33.1	117	85.0
^{32}S + ^{32}S	2021	7.36	7.36	16.3	64.9	48.9

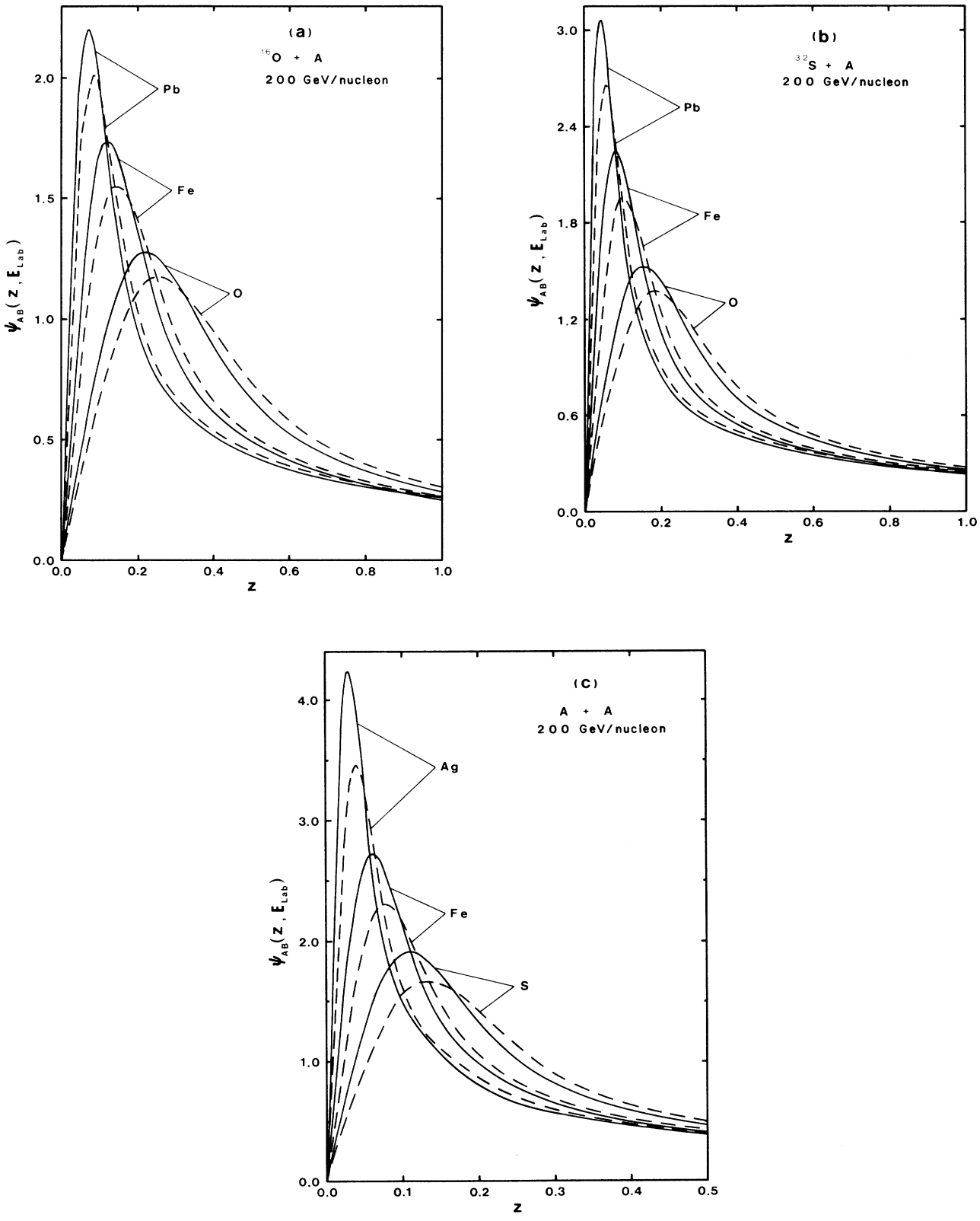

FIG. 1. Predicted KNO function for nucleus-nucleus collisions at 200 GeV/nucleon. Calculations for the cases MCM and WNM are shown by solid and dashed curves, respectively. The nuclide A is indicated on the side of curves.

(c) We use[18] $\sigma_{\text{inel}}^{NN}=32.1$ mb for $E_{\text{lab}}=200$ GeV/nucleon and $\sigma_{\text{inel}}^{NN}=31.7$ mb at $E_{\text{lab}}=15$ GeV/nucleon in Eqs. (2.12) and (2.14)–(2.16).

(d) In Eq. (2.13), we adopt $\rho_A(r)$ as given in Ref. 19:

$$\rho_A(r)=\rho_0[1+\exp(r-R_A)/d]^{-1}\ ,$$
$$R_A=(1.19A^{1/3}-1.61A^{-1/3})\ \text{fm}\ , \tag{3.4}$$
$$d=0.54\ \text{fm}\ ,$$

where ρ_0 is determined from the normalization. This parametrization provides, via the Glauber formula, a satisfactory agreement between the calculated and measured hadron-nucleus reaction cross sections.[19] Note that the usage of a realistic ρ_A is important for the calculations of $\psi_{AB}(z,E_{\text{lab}})$ at small z, since, in this case, contributions from large b_I become dominant.

We show in Table I the calculated value of σ_{abs}^{AB} for various AB collisions at $E_{\text{lab}}=200$ and 15 GeV/nucleon together with $\langle w_A\rangle$, $\langle w_B\rangle$, and $\langle N_{Ab}\rangle$, which are obtained by averaging $\langle w_A(b_I)\rangle$, $\langle w_B(b_I)\rangle$, and $\langle N_{AB}(b_I)\rangle$ over b_I with the weight $\sigma_{\text{abs}}^{AB}(b_I)/\sigma_{\text{abs}}^{AB}$. Also shown are the values of $\langle n(E_{\text{lab}})\rangle_{AB}$ calculated from Eqs. (2.6), (2.8), and (2.9) for WNM and MCM. From this table, we observe that MCM gives $\langle n(E_{\text{lab}})\rangle_{AB}$ 30–45% larger at 200 GeV/nucleon and 10–30% smaller at $E_{\text{lab}}=15$ GeV/nucleon, compared with those given in WNM. The simplest version of the energy partition in the MCM Eq. (2.9) underestimates $\langle n(E_{\text{lab}})\rangle_{AB}$ at lower energy,[20] although the b_I dependence of $\langle n(b_I,E_{\text{lab}})\rangle_{AB}$ is not expected to change much if more sophisticated versions of the energy partition are used. A constant multiplied to $\langle n(b_I,E_{\text{lab}})\rangle_{AB}$ does not affect the results on $\psi_{AB}(z,E_{\text{lab}})$ given below.

B. KNO function of AB collisions

We show the prediction of our model for $\psi_{AB}(z,E_{\text{lab}})$ of the charged secondary multiplicity distributions for various combinations of A and B colliding at $E_{\text{lab}}=200$ GeV/nucleon in Figs. 1(a)–1(c). Results are shown only for the region $z\leq 1.0$ in Figs. 1(a) and 1(b) and for $z\leq 0.5$ in Fig. 1(c) to illustrate the peaks of $\psi_{AB}(z,E_{\text{lab}})$ on a linear scale. It can be seen that the difference between case MCM (solid curves) and case WNM (dashed curves) for each $A+B$ is significant only in the peak region. Case MCM gives a higher peak and the position of the peak is situated at a smaller z as compared with case WNM. For both cases, the peak is generally higher and the position of the peak occurs at smaller z when the combination A and B gives larger $\langle N_{AB}\rangle$. This trend of nuclear-mass number dependence of the peak is consistent with that observed in pA collisions.[12–14]

As mentioned in the previous section, values of $\psi_{AB}(z,E_{\text{lab}})$ calculated for case WNM, approximately scale with energy and its change is negligible for the range of energy interested in this paper. For case MCM, however, considerable energy dependence exists in the peak region. To see this, we show $\psi_{AB}(z,E_{\text{lab}})$ in case-MCM for collisions of ^{32}S off ^{16}O, Fe, and Pb at $E_{\text{lab}}=15$ GeV/nucleon in Fig. 2. Comparing Figs. 1(b)

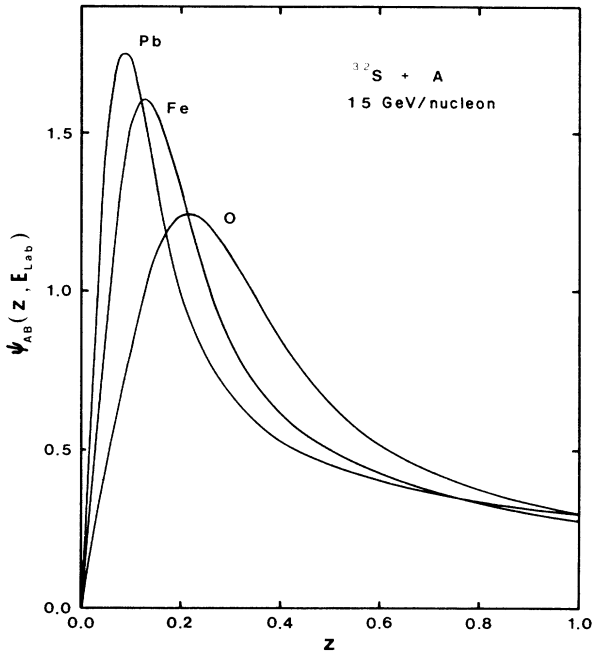

FIG. 2. Predicted KNO function for ^{32}S + A collisions at 15 GeV/nucleon for the case MCM. The nuclide A is shown on the side of curves.

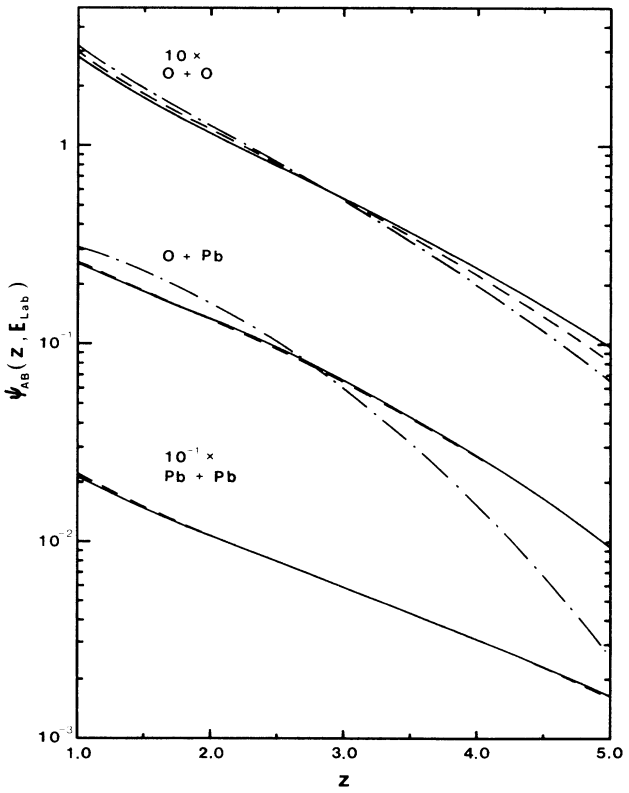

FIG. 3. Predicted KNO function for nucleus-nucleus collisions at large z. Solid (dashed) curves show the case MCM (WNM) at 200 GeV/nucleon and dash-dot curves show the case MCM at 15 GeV/nucleon.

and 2, we observe that the peak is higher and the position of the peak is located at a smaller z when $E_{\rm lab}$ is larger. We summarize our result on the normalized moments $c_m = \langle n^m \rangle_{AB} / \langle n \rangle_{AB}^m$ for $m = 2$, 3, 4 at both energies in Table II.

We turn to the large-z ($\gtrsim 1.5$) region where signals of new phenomena such as QGP formation might be expected directly in the multiplicity distribution, or the multiplicity may be used as a trigger for other signals. We note that we need the information on $\psi(\tilde{z})$ only for $\tilde{z} \lesssim 2.5$ to calculate $\psi_{AB}(z, E_{\rm lab})$ up to $z = 5$ because $Q_{AB}^{-1}(b, E_{\rm lab})$ in Eq. (2.5) is less than 0.5 at $b = 0$ for A and B listed in Tables I and II. In Fig. 3 we show our calculation of $\psi_{AB}(z, E_{\rm lab})$ at $1 \le z \le 5$ for ^{16}O + ^{16}O, ^{16}O + Pb, and Pb + Pb collisions at $E_{\rm lab} = 200$ GeV/nucleon. For the former two cases, we also show the result of case MCM at $E_{\rm lab} = 15$ GeV/nucleon. At 200 GeV/nucleon, case MCM and case WNM show little difference for each $A + B$ collision. One can easily confirm this result also for other combinations of A and B listed in Tables I and II. The dependence of $\psi_{AB}(z, E_{\rm lab})$ on A and B in this region of z is much less pronounced than that in the peak region.

IV. DISCUSSION

The main features of our model can be summarized as follows.

(a) The peak height and the position of $\psi_{AB}(z, E_{\rm lab})$ depend strongly on $\langle N_{AB} \rangle$. This dependence on $\langle N_{AB} \rangle$ is similar both for case MCM and case WNM. Thus, independent of the use of MCM or WNM, our model can be tested against experiments by comparing the movement of the peak when A and B are varied.

(b) In the peak region ($z \lesssim 1$), the factorizable and unfactorizable forms of $\langle n(b_I, E_{\rm lab}) \rangle_{AB}$ lead to a totally different energy dependence of $\psi_{AB}(z, E_{\rm lab})$. Thus, measurement on $\psi_{AB}(z)$ in the region $z \lesssim 1$ at different energies will distinguish clearly the forms of $\langle n(b_I, E_{\rm lab}) \rangle_{AB}$, especially for large $\langle N_{AB} \rangle$.

(c) In the tail region ($z \gtrsim 1$), our model provides a unique prediction of $\psi_{AB}(z)$ at $E_{\rm lab} = 200$ GeV/nucleon for each A and B. It is not sensitive to the particular choice of the input $\langle n(b_I, E_{\rm lab}) \rangle_{AB}$ at $E_{\rm lab} = 200$ GeV/nucleon.

We would like to comment on the two models for $\langle n(b_I, E_{\rm lab}) \rangle_{AB}$. In a recent experiment,[4] the charged multiplicity $N_{\pm}$ at laboratory angles $\theta < 60°$ in ^{16}O + Pb collisions at 200 GeV/nucleon was observed as a function of the total energy $E_{\rm veto}$ in the forward veto calorimeter. We assume that the observed charged particles are the charged secondary particles and the beam spectator protons. Suppose we identify $E_{\rm veto}/200$ GeV as the number of beam spectator nucleons in ^{16}O, $\langle s_{\rm O}(b_I) \rangle = 16 - \langle w_{\rm O}(b_I) \rangle$, we obtain a relation between

TABLE II. Results for scaled moments c_m for lower m's at 200 GeV/nucleon calculated for the cases MCM and WNM. Values in parentheses are those at 15 GeV/nucleon.

	MCM			WNM		
$A + B$	c_2	c_3	c_4	c_2	c_3	c_4
^{16}O + ^{207}Pb	2.32 (1.95)	8.11 (5.50)	40.7 (21.9)	2.31 (2.30)	8.17 (8.07)	41.7 (40.9)
^{16}O + ^{108}Ag	2.40 (2.06)	8.95 (6.36)	48.6 (28.1)	2.34 (2.33)	8.61 (8.51)	46.2 (45.4)
^{16}O + ^{56}Fe	2.42 (2.12)	9.40 (6.97)	53.6 (33.4)	2.33 (2.31)	8.67 (8.57)	47.7 (46.8)
^{16}O + ^{16}O	2.22 (2.00)	8.06 (6.37)	43.8 (30.3)	2.10 (2.08)	7.18 (7.05)	36.7 (35.7)
^{32}S + ^{207}Pb	2.54 (2.06)	9.95 (6.21)	56.2 (26.4)	2.51 (2.50)	9.80 (9.73)	55.7 (55.1)
^{32}S + ^{108}Ag	2.64 (2.20)	11.0 (7.32)	67.0 (35.1)	2.55 (2.54)	10.3 (10.3)	61.3 (60.9)
^{32}S + ^{56}Fe	2.65 (2.26)	11.3 (8.00)	71.5 (41.4)	2.52 (2.51)	10.3 (10.2)	61.8 (61.4)
^{32}S + ^{16}O	2.38 (2.11)	9.19 (7.03)	52.8 (34.7)	2.26 (2.24)	8.27 (8.16)	45.0 (44.1)
^{207}Pb + ^{207}Pb	2.90	13.4	91.0	2.84	12.9	86.5
^{108}Ag + ^{108}Ag	2.87	13.2	89.8	2.77	12.3	80.6
^{56}Fe + ^{56}Fe	2.76	12.3	81.0	2.63	11.1	69.9
^{32}S + ^{32}S	2.57	10.8	67.0	2.44	9.64	56.7

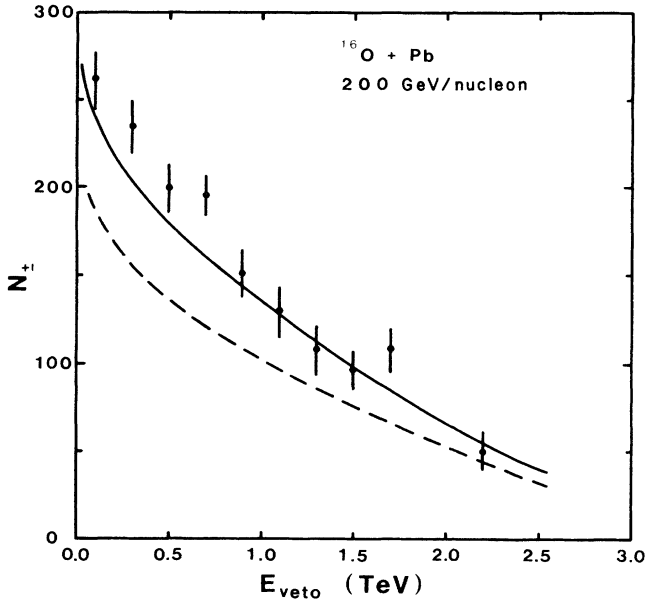

FIG. 4. Mean charged-particle multiplicity as a function of the total energy in the forward veto calorimeter. Solid and dashed curves are calculated by the MCM and WNM, respectively. Data are taken from Ref. 4.

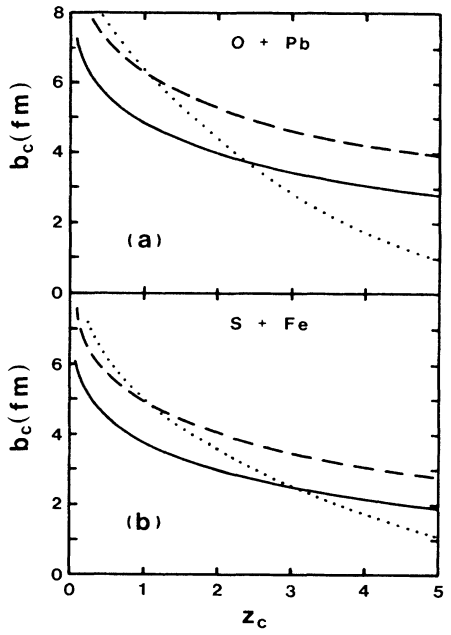

FIG. 5. Impact-parameter cut as a function of the multiplicity cut for 200-GeV/nucleon nucleus-nucleus collisions. Solid and dashed curves are for $r_c=0.5$ and 0.8, respectively. Dotted curves show the geometric estimate.

$E_{\rm veto}$ and b_I. Using this relation, we plot $N_{\pm}=\langle n(b_I,E_{\rm lab})\rangle_{\rm O\,Pb}+\langle s_{\rm O}(b_I)\rangle/2$ as a function of $E_{\rm veto}$ together with the experimental data in Fig. 4. The solid curve calculated from the MCM reproduces the experimental data well. Deviation of the curves from the experimental data at $E_{\rm veto}<0.8$ TeV may be explained as the effect of particle production due to the internuclear cascading in the target nucleus (Pb). The deviation from the experimental data in the small $E_{\rm veto}$ region is larger for the dashed curve which is calculated from the WNM. Although the result may suggest that the MCM is preferable, we do not go further on this point because our assumption regarding the relation between b_I and $E_{\rm veto}$ may be oversimplified.

Since our model is based on geometric aspects, we can relate the cut in the multiplicity with that in the impact parameter. To do this, we calculate the probability r_c that an $A+B$ collision takes place at the impact parameter $b_I<b_c$ among events with a scaled multiplicity $z>z_c$:

$$r_c=\Phi_{AB}^{-1}(z_c)\int_0^{b_c}2\pi b_I db_I\frac{\sigma_{\rm abs}^{AB}(b_I)}{\sigma_{\rm abs}^{AB}}\Phi_{AB}(z_c,b_I)\ , \tag{4.1}$$

where

$$\Phi_{AB}(z_c,b_I)=\sum_n\theta(n-z_c\langle n(E_{\rm lab})\rangle_{AB})\times P_n^{AB}(b_I,E_{\rm lab})\ ,$$

$$\Phi_{AB}(z_c)=\int d^2\mathbf{b}_I\frac{\sigma_{\rm abs}^{AB}(b_I)}{\sigma_{\rm abs}^{AB}}\Phi_{AB}(z_c,b_I)\ .$$

In Figs. 5(a) and 5(b), we show the values of b_c as a function of z_c at $r_c=0.5$ and 0.8 for ^{16}O + Pb and ^{32}S + Fe collisions, respectively, at $E_{\rm lab}=200$ GeV/nucleon. We used the MCM for $\langle n(b_I,E_{\rm lab})\rangle_{AB}$ in this calculation. The difference between case WNM and case MCM is less than 5%. For comparison, we also show the geometric estimate of b_c:

$$\sigma_{\rm abs}^{AB}\Phi_{AB}(z_c)=\int_0^{b_c}2\pi b_I db_I\sigma_{abs}^{AB}(b_I)\ . \tag{4.2}$$

Our illustration shows, for example, for the multiplicity cut at $z_c=3$ in ^{16}O + Pb collisions, that 50% of the events occur with $b_I<3.5$ fm, and 80% of the events occur with $b_I<4.5$ fm. For collisions of $A+B$ with $\langle N_{AB}\rangle=20$–30 at $E_{\rm lab}=200$ GeV/nucleon, the geometric estimate in the region $1<z_c<3$ can be regarded as providing a b_c for which approximately 50–80% of the events occur with $b<b_c$. Such information would be valuable for a comparison of the theoretical calculation with experiments concerning the signals of the QGP.

ACKNOWLEDGMENTS

This work was partly supported by an operating grant from the Natural Sciences and Engineering Council of Canada. C.K.C. acknowledges the hospitality of the International Centre for Theoretical Physics, Trieste, Italy. S.D. is grateful to the Killam Trustee for financial support and F. Takagi for useful correspondence.

*Permanent address: Department of Physics, National University of Singapore, Singapore, 0511.

[1]*Proceedings of the Fourth International Conference on Ultrarelativistic Nucleus-Nucleus Collisions,* Helsinki, 1984, edited by K. Kajantie (Springer, Berlin, 1985).

[2]*Proceedings of the Fifth International Conference on Ultrarelativistic Nucleus-Nucleus Collisions,* Asilomar, 1986, edited by L. S. Schroeder and M. Gyulassy [Nucl. Phys. **A461** (1987)].

[3]*Proceedings of the Second International Conference on Nucleus-Nucleus Collisions,* Visby, Sweden, 1985, edited by H.-Å. Gustafsson, B. Jakobsson, I. Otterlund, and K. Alekleth [Nucl. Phys. **A447** (1986)].

[4]A. Bamberger *et al.*, Phys. Lett. B **184**, 271 (1987).

[5]T. H. Burnett *et al.*, Phys. Rev. Lett. **50**, 2062 (1983); F. Takagi, *ibid.* **53**, 427 (1984).

[6]G. Baym, in *Proceedings of the Fourth International Conference on Ultrarelativistic Nucleus-Nucleus Collisions* (Ref. 1).

[7]A. Capella and A. Krzywicki, Phys. Rev. D **18**, 3357 (1978); K. Kinoshita, A. Minaka, and H. Sumiyoshi, Prog. Theor. Phys. **61**, 165 (1979).

[8]H. Sumiyoshi, Phys. Lett. **131B**, 241 (1983).

[9]A. Białas, M. Bleszyński, and W. Czyż, Nucl. Phys. **B111**, 461 (1976).

[10]I. Otterlund and E. Stenlund, Phys. Scr. **22**, 15 (1980).

[11]J. P. Vary, Phys. Rev. Lett. **40**, 295 (1978); F. Takagi, Prog. Theor. Phys. **71**, 585 (1984).

[12]D. Kiang, S. H. Ling, K. Young, and C. S. Lam, Phys. Rev. D **31**, 31 (1985).

[13]C. De Marzo *et al.*, Phys. Rev. D **26**, 1019 (1982).

[14]N. N. Biswas *et al.*, Phys. Rev. D **33**, 3167 (1986).

[15]K. Kinoshita, A. Minaka, and H. Sumiyoshi, Z. Phys. C **8**, 205 (1981).

[16]P. Slattery, Phys. Rev. Lett. **29**, 1624 (1972).

[17]W. Thomé *et al.*, Nucl. Phys. **B129**, 365 (1977).

[18]J. Whitmore, Phys. Rep. **C23**, 286 (1976).

[19]S. Daté, H. Sumiyoshi, and M. Gyulassy, Phys. Rev. D **32**, 619 (1985).

[20]H. Sumiyoshi (private communication).